Airborne Magnetic Technoparticles in Soils as a Record of Anthropocene

Wanda Wilczyńska-Michalik [1,*], **Jan M. Michalik** [2], **Czesław Kapusta** [2] **and Marek Michalik** [3]

1   Institute of Geography, Pedagogical University of Krakow, ul. Podchorazych 2, 30-084 Krakow, Poland
2   Department of Solid State Physics, Faculty of Physics and Applied Computer Science, AGH University of Science and Technology, al. A. Mickiewicza 30, 30-059 Krakow, Poland; jmichali@agh.edu.pl (J.M.M.); kapusta@agh.edu.pl (C.K.)
3   Institute of Geological Sciences, Jagiellonian University, ul Gronostajowa 3a, 30-387 Krakow, Poland; marek.michalik@uj.edu.pl
*   Correspondence: wanda.wilczynska-michalik@up.krakow.pl

check for updates

Abstract: Airborne magnetic particles in soils were studied in sites located in various distances to industrial plants. Chemical and mineral composition of soil samples were analysed. The highest values of the Pollution Load Index (PLI) calculated for several elements were noted for sites relatively distant from industrial plants. Soil samples exposed for the deposition of airborne particles were examined by means of magnetization versus an external applied magnetic field as well as ^{57}Fe Mössbauer spectroscopy measurements showing a lack of correlation of the magnetic properties with total Fe content, which points toward a strong impact of the industrial activities. Magnetic fraction was extracted and studied using scanning electron microscopy with energy dispersive spectrometry. Two types of spherical particles were noted. Massive ones occurring in all sites and particles with a complex internal structure more abundant in sites situated closer to industrial plants. The presence of spherical magnetic particles formed in high temperature processes indicate their relatively long range transport in the atmosphere. Broad distribution, characteristic and easy for identification spherical form of these magnetic technoparticles, suggest that one can consider them as a record of the Anthropocene. Accumulation of such technoparticles is related to rapid industrialization in the post-World War II period.

Keywords: airborne magnetic technoparticles; magnetometry; Mössbauer spectroscopy; soil pollution; record of Anthropocene

1. Introduction

The Anthropocene is defined as an epoch of significant human impact on the Earth ecosystems [1,2]. Various dates of the beginning of the Anthropocene have been proposed and different records of the Anthropocene were discussed [3]. The Anthropocene epoch is characterized by the production of numerous human-made materials [4], which could be dispersed in sediments as technofossils [5]. The dispersion of fragments of human-made materials (technoparticles) in sediments is controlled by the mechanism of their transport. River flow results in the deposition of technoparticles in fluvial sediments and ocean currents disperse technoparticles in ocean sediments. Dispersion of small particles in the atmosphere is very effective on a global scale similarly to aeolian transport of natural dust [6].

Variation of chemical pollutants' concentration in soil profiles, isotopic signatures, magnetic properties of soils and sediments, and presence of technofossils are often considered as markers of the Anthropocene [7–11].

Our study is focused on the identification of magnetic technoparticles in the soils of Southern Poland collected from sites in various distances from industrial sources of air pollution, analysis of magnetic properties, and chemical composition of soils, and on interpretation of interrelationships between these parameters. Soil profiles exposed to the deposition of airborne particles were selected. Selected soil profiles are devoid of any direct influx of anthropogenic material (e.g., from situated nearby industrial waste disposal sites).

Magnetic technoparticles in soils could be considered as a record of the Anthropocene [12,13] easy for identification using the scanning electron microscope fitted with X-ray energy dispersive spectrometer (SEM-EDS) and extraction from soil samples using the hand magnet or simple separators.

Particulate matter (PM) in the air in Southern Poland, emitted from numerous sources (e.g., household coal and wood burning, vehicular emission, industrial plants, soil erosion, and resuspension) is composed of soot, silicate, and aluminosilicate particles, metallic or metal oxide particles, sulphates, and chlorides. Clear recognition of PM sources is often problematic.

The topsoil magnetic properties due to a presence of magnetic particles can be easily measured by a low-field room temperature magnetic susceptibility. Magnetic particles can be either naturally present in the soil of anthropogenic origin i.e., deposited mainly from the atmosphere [14–18]. In both cases, they undergo important modifications due to environmental conditions [19–21]. Therefore, for the proper interpretation of the magnetic susceptibility data, a more detailed study is required, including low temperature susceptibility measurements as well as temperature-dependent studies. Such data reveal different coupling types between magnetic moments and their strength and, consequently, allows a deeper insight into the type of magnetic species present in the magnetic particles. Not less importantly, ^{57}Fe Mössbauer spectroscopy measurements both at room temperatures and (for selected samples) at liquid Helium temperatures, give detailed information on the oxidation state of Fe in the compound, as well as on the local ordering of the material. With respect to that, Mössbauer hyperfine parameters are a kind of fingerprint allowing a precise determination of the sample composition [22–26]. Combining magnetization data with these obtained from spectroscopic measurements gives a perfect opportunity to clearly distinguish particles coming from different anthropogenic sources. This is due to the fact that anthropogenic magnetic particles differentiate from the natural ones not only by their specific morphology [27] but also by the very distinct magnetic properties. They usually occur as the ferrimagnetic phases of Fe oxides, i.e., magnetite and maghemite, with Fe ions very often substituted by other cations.

2. Experiments

Among sampling sites, 20 samples from 10 different sites were collected. Eight samples were collected from four sites situated in the northeastern outskirts of Krakow, where industrial plants are concentrated. Other sampling sites were situated in various distances to the main industrial sources of emission (for two sites, the distance was from 10 to 20 km and for the other four above 35 km) (see Figure 1 for localisation names and symbols of samples). It is worthy to mention that western wind dominate in the area of Krakow [28]. The Krakow Steel Plant was constructed in the 1950s. The highest steel production was reached in the 1970s (6,700,000 tonnes of steel in 1977). The highest emission of dust was 104,000 tonnes (in 1974), and of sulphur dioxide was 70,000 tonnes in 1974 [29]. Coal burning Power Plant in Łęg (eastern margin of Krakow) is equipped with pulverised fuel boilers and represents the other important industrial source of pollution in this area. Other industrial area is situated near Skawina where the coal burning power plant is the main source of dust emission (Figure 1).

Samples at each site were collected from two depth horizons: 0–10 cm and 20–40 cm. Sample symbols indicate depth horizon, i.e., sample with index "1"after the localisation symbol was collected from 0–10 cm in depth, and sample with index "2"after the localisation symbol from 20–40 cm in depth.
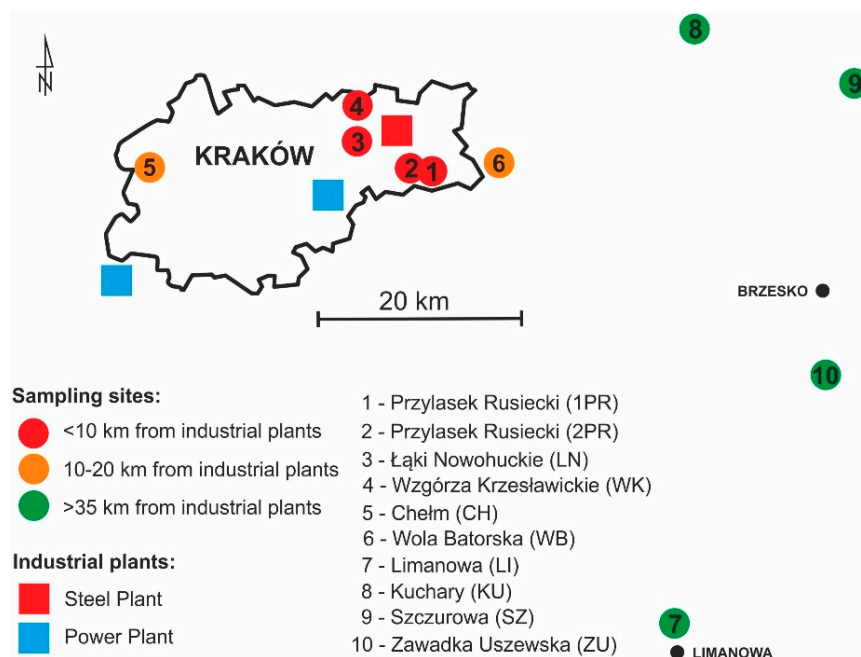
Figure 1. Localisation of sampling sites and main industrial sources of dust emission.

Mineral composition of soils and separated magnetic fractions was determined using powder X-ray diffractometry (XRD). Philips X-ray diffractometer equipped with vertical goniometer with graphite curved crystal monochromator was used. X-ray diffraction patterns were collected using CuKα radiation. Samples were prepared by grinding of soil samples in a hand mortar.

The chemical composition of soil samples was analyzed using ICP AES (Inductively Coupled Plasma Atomic Emission Spectrometry) and ICP MS (Inductively Coupled Plasma Mass Spectrometry) methods for major and trace elements in the Bureau Veritas (former AcmeLabs, Vancouver, Canada). Loss of ignition (LOI) was determined by the mass difference after heating to 1000 °C, while the Leco method was used for determining total C and S content.

The magnetic fraction was separated from soil material sieved through a 1-mm sieve after crushing using wooden and porcelain tools. Fraction <1 mm was subjected to extraction of magnetic components in water, using neodymium magnet with B = 0.25 T at its surface, as measured with a standard laboratory Gauss meter.

Magnetic fraction was prepared for microscopic observation as polished thin sections after impregnation in resin.

Both optical microscope and scanning electron microscope were used for magnetic fraction observations. Field emission scanning electron microscope (FE-SEM) HITACHI S-4700 was equipped with X-ray energy dispersive spectrometer (EDS) NORAN NSS. The standard-less method was applied for chemical elements quantification.

Magnetic isothermal loops M(H) at room temperature were collected in a range up to 10 kOe using the Lake Shore Vibrating Sample Magnetometer (VSM) Cryotronics Inc. model 7300 (Westerville, OH, USA). The temperature stability was monitored during the measurements. The isothermal loops at temperatures ranging from 4 K to 300 K and magnetic field up to 90 kOe as well as zero field cooled (ZFC) and field cooled (FC) magnetic susceptibility curves were measured for selected samples with the Vibrating Sample Magnetometer option of a Quantum Design Physical Properties Measuring System.

Samples for Mössbauer spectroscopy measurements were prepared using 200 mg of the material formed into a 12-mm diameter powder absorbent. [57]Fe Mössbauer measurements were carried out in the transmission mode with a constant acceleration spectrometer. A source of 50 mCi [57]Co in the rhodium matrix was used. Low-temperature measurements were carried out in a cold finger type

cryostat, filled with liquid nitrogen or helium. The spectra obtained were fitted using Gauss–Newton's iterative method of minimizing chi^2, with a Lorentzian shape of the spectral lines.

3. Results and Discussion

3.1. Mineral Composition of Soil Samples

X-ray diffraction analysis indicates that the mineral composition of the bulk samples from the two depth horizons for each site is similar. The mineral composition of the samples from the different sites is also very similar. Quartz dominates and is accompanied by subordinate feldspars, mica, and clay minerals. The samples from Limanowa and Szczurowa are enriched in clay minerals, while the sample from the lower horizon from Wzgórza Krzesławickie contains a small amount of dolomite.

3.2. Chemical Composition of Soil Samples

Results from the chemical analysis of the bulk soil samples (Table 1) show that the content of SiO_2 varies from 55 to 84 wt%. Al_2O_3 from 4 to 15 wt%, and Fe_2O_3 from 1.5 to 7.2 wt%. The highest content of Fe is noted in the samples from Szczurowa and Limanowa representing sites distant from the Steel Plant. The lowest in samples is from Łąki Nowohuckie and Chełm. The Fe content in the samples is partly correlated with Al_2O_3 and likely related to the content of clay minerals. The content of heavy metals (Table 2) in all samples is below the allowable limits for agricultural soils, according to Polish regulations, except for that of Ba for all samples and Co for one sample (SZ2), where the content is slightly above this limit. It is possible to notice that the content of trace elements is not related to the distance of industrial plants (Table 2, Figure 1).

Table 1. Major chemical components in soil samples (Ctot and Stot—total content of C and S).

Sample	Component (wt%)													
	SiO2	Al2O3	Fe2O3	MnO	MgO	CaO	Na2O	K2O	TiO2	P2O5	LOI	Total	Ctot	Stot
1PR1	73.31	7.60	3.17	0.09	0.59	1.10	0.80	2.19	0.64	0.30	10.10	99.89	3.72	0.04
1PR2	76.25	7.69	3.10	0.10	0.58	1.25	0.83	2.19	0.65	0.26	6.80	99.7	2.07	0.03
2PR1	65.34	7.58	3.71	0.08	0.65	1.57	0.76	1.89	0.57	0.22	17.4	99.77	6.63	0.09
2PR2	74.02	8.30	2.94	0.04	0.58	1.07	0.84	1.86	0.64	0.14	9.30	99.73	2.29	0.03
WK1	78.83	7.58	2.63	0.07	0.50	0.66	0.81	2.11	0.67	0.12	5.80	99.78	2.72	0.03
WK2	76.56	7.21	2.67	0.06	0.47	0.69	0.78	2.02	0.66	0.14	8.50	99.76	1.50	<0.02
LN1	83.83	3.91	1.94	0.03	0.26	0.57	0.31	1.00	0.28	0.12	7.60	99.85	3.05	0.04
LN2	84.21	4.76	1.95	0.03	0.30	0.60	0.36	1.12	0.35	0.1	6.10	99.88	1.99	0.03
CH1	81.81	6.34	1.67	0.06	0.34	0.37	0.74	1.92	0.65	0.12	5.70	99.72	1.71	<0.02
CH2	83.73	6.51	1.59	0.06	0.35	0.38	0.75	1.92	0.67	0.08	3.70	99.74	0.78	<0.02
WB1	74.42	8.27	2.84	0.09	0.62	0.47	0.91	1.79	0.67	0.15	9.60	99.83	2.69	0.03
WB2	76.79	9.02	3.11	0.10	0.69	0.45	1.00	1.99	0.74	0.16	5.80	99.85	0.95	<0.02
SZ1	55.82	13.30	7.11	0.26	1.08	0.62	0.53	1.74	0.74	0.20	18.40	99.8	3.96	0.05
SZ2	62.47	14.12	7.19	0.45	1.17	0.75	0.65	2.14	0.76	0.09	10.00	99.79	0.73	<0.02
KU1	72.14	8.22	2.82	0.06	0.72	1.53	0.82	2.31	0.67	0.20	10.30	99.79	3.48	0.04
KU2	76.16	8.52	2.88	0.06	0.74	1.20	0.83	2.34	0.69	0.16	6.20	99.78	1.81	0.02
LI1	65.88	13.63	4.94	0.10	1.50	0.46	1.17	2.63	0.93	0.13	8.40	99.77	1.79	0.03
LI2	63.99	15.50	6.29	0.19	1.83	0.37	1.21	3.00	0.86	0.08	6.50	99.82	0.54	<0.02
ZU1	78.48	7.84	2.32	0.06	0.53	0.41	0.80	2.10	0.69	0.09	6.50	99.82	1.72	0.02
ZU2	79.73	8.38	2.47	0.08	0.56	0.43	0.85	2.23	0.76	0.10	4.20	99.79	0.66	<0.02

Table 2. Trace elements content in soil samples (in ppm, except of Au in ppb) and PLI values (Pollution Load Index).

Sample	Ag	As *	Au **	Ba	Be	Bi	Cd *	Co *	Cr *	Cs	Cu *	Ga	Hf	Hg	Mo	Nb	Ni *	Pb *	Rb	Sb	Sc	Se	Sn	Sr
1PR1	<0.1	3.8	4.1	435	<1	0.2	0.8	5.7	55.71	2.60	29.20	7.10	13.40	0.05	0.4	11.3	16.4	27.4	78.4	0.3	7	<0.5	2	84.5
1PR2	<0.1	4.6	1.9	439	2	0.2	1.1	6.7	61.90	3.00	32.20	7.70	14.00	0.06	0.3	12.4	16.9	32.0	86.6	0.3	7	<0.5	3	96.4
2PR1	<0.1	4.6	5.7	389	1	0.2	1.4	6.0	74.29	2.60	19.10	7.60	10.10	0.07	0.4	10.7	16.9	41.8	66.2	0.4	7	<0.5	2	86.8
2PR2	<0.1	4.6	5.0	429	<1	0.1	0.6	6.3	61.90	3.00	14.70	7.80	13.80	0.04	<0.1	12.5	17.6	24.9	64.5	0.2	7	<0.5	2	89.9
WK1	<0.1	4.4	4.1	426	1	0.1	0.7	7.4	49.52	2.60	14.90	7.20	15.00	0.05	0.3	13.0	13.5	27.6	75.0	0.4	7	0.7	2	89.2
WK2	<0.1	5.0	9.7	428	<1	0.2	1.2	6.5	49.52	2.50	16.30	6.70	14.90	0.07	0.4	13.1	13.2	35.2	72.4	0.4	6	<0.5	2	88.8
LN1	<0.1	4.8	3.7	244	2	0.1	0.8	3.9	43.33	1.60	9.30	2.80	5.60	0.04	0.3	5.3	7.5	29.2	34.1	0.9	3	<0.5	1	48.4
LN2	0.1	5.2	2.3	262	<1	<0.1	0.7	4.7	30.95	1.50	10.30	4.60	6.50	0.03	0.1	6.5	9.5	26.5	39.9	0.5	4	<0.5	2	52.0
CH1	<0.1	3.1	2.8	363	2	0.1	0.7	4.9	61.90	1.90	6.60	6.10	15.80	0.03	0.2	12.0	7.5	27.6	64.5	0.2	5	0.5	2	69.6
CH2	<0.1	2.6	2.2	370	<1	0.1	0.7	4.2	55.71	1.70	6.00	5.60	15.60	0.03	0.2	12.2	7.8	23.1	64.5	0.2	5	<0.5	1	69.5
WB1	0.1	5.3	4.1	387	2	0.2	0.9	6.7	74.29	3.00	15.50	8.50	11.80	0.07	0.30	12.90	26.00	34.00	87.6	0.30	7	<0.5	3	72.6
WB2	<0.1	5.1	3.1	433	<1	0.2	0.7	8.2	80.48	3.50	14.50	9.60	11.80	0.05	0.20	14.10	29.00	27.30	92.4	0.20	8	<0.5	2	79.3
SZ1	0.1	15.2	4.9	414	2	0.4	0.6	15.7	80.48	7.40	19.90	15.80	6.40	0.07	0.90	13.80	35.00	44.00	131.7	0.20	12	1	3	80.3
SZ2	<0.1	11.6	6.4	518	<1	0.3	0.4	24.5	80.48	7.40	24.60	16.30	8.80	0.06	0.80	14.40	46.00	21.90	122.7	0.10	13	0.8	3	89.5
KU1	<0.01	4.8	14.5	386	2	0.1	0.5	6.8	55.71	2.80	16.50	8.30	14.70	0.04	0.40	12.30	22.00	26.20	78.7	0.30	7	0.7	2	86.9
KU2	<0.01	5.6	2.3	403	2	0.2	0.5	7.1	55.71	3.00	14.70	9.40	15.30	0.05	0.20	13.40	22.00	22.90	86.4	0.20	7	0.5	2	85.1
LI1	<0.1	6.0	4.1	457	<1	0.3	0.6	14.9	92.86	5.60	23.10	15.50	8.40	0.09	0.7	17.5	37.9	31.5	116.5	0.2	13	0.6	3	99.5
LI2	<0.1	8.7	21.9	459	4	0.3	0.2	20.4	99.05	5.90	33.50	18.00	7.10	0.04	0.8	15.4	49.9	24.9	127.2	0.2	15	<0.5	3	89.9
ZU1	<0.1	5.2	3.7	409	<1	0.2	0.2	6.6	55.71	2.80	10.60	8.70	16.10	0.07	0.30	13.80	<20	17.80	82.3	0.20	6	<0.5	2	78.9
ZU2	<0.1	4.1	3.8	431	2	0.1	0.2	6.9	55.71	3.00	9.20	8.30	17.10	0.04	0.50	15.00	21.00	16.40	85.9	0.20	7	<0.5	2	79.4

Table 2. *Cont.*

Sample	Ta	Th	Tl	U	V	W	Y	Zn *	Zr	La	Ce	Pr	Nd	Sm	Eu	Gd	Tb	Dy	Ho	Er	Tm	Yb	Lu	PLI ***
1PR1	<0.1	9.1	0.2	2.7	52.0	1.7	24.0	140	500.1	27.6	56.8	6.93	26.00	4.89	0.80	4.35	0.72	4.40	0.84	2.53	0.41	2.68	0.46	**1.055**
1PR2	<0.1	8.9	0.2	2.8	51.0	2.1	27.0	156	545.9	29.5	59.1	6.94	26.50	5.04	0.94	4.85	0.80	4.75	0.91	2.81	0.43	3.02	0.47	**1.221**
2PR1	<0.1	8.5	0.1	2.4	49.0	1.4	23.7	176	394.6	24.3	50.9	6.06	21.70	4.74	0.85	4.32	0.72	3.92	0.78	2.54	0.39	2.63	0.42	**1.249**
2PR2	<0.1	10.4	<0.1	2.9	51.0	1.3	25.9	80	526.9	28.8	59.5	6.90	25.20	4.99	0.93	4.93	0.78	4.49	0.89	2.83	0.44	2.94	0.46	0.913
WK1	<0.1	9.4	0.2	3.0	48.0	1.6	27.4	101	594.2	28.7	58.4	6.69	25.80	4.89	0.86	4.73	0.77	4.66	0.96	3.18	0.49	3.19	0.51	0.928
WK2	<0.1	9.2	0.2	3.3	46.0	3.1	26.9	139	578.1	26.8	58.5	6.82	26.10	5.05	0.84	4.73	0.80	4.67	0.89	2.99	0.46	3.16	0.49	**1.074**
LN1	<0.1	4.2	<0.1	1.6	23.0	1.8	11.5	124	213.6	12.3	26.2	2.86	11.10	2.22	0.38	1.98	0.32	1.81	0.38	1.19	0.19	1.34	0.21	0.784
LN2	0.1	5.3	<0.1	1.7	31.0	0.7	13.2	83	253.7	15.9	32.0	3.61	12.50	2.39	0.46	2.28	0.39	2.15	0.45	1.37	0.21	1.48	0.22	0.749
CH1	<0.1	9.4	0.2	3.0	45.0	1.3	22.7	62	592.0	25.2	53.9	5.93	22.00	4.59	0.67	3.58	0.64	3.86	0.82	2.49	0.43	2.73	0.45	0.685
CH2	<0.1	9.3	0.1	2.8	36.0	2.3	22.5	64	601.2	24.9	51.8	5.71	20.20	4.06	0.66	3.78	0.63	3.96	0.80	2.67	0.38	2.66	0.43	0.632
WB1	0.1	10.1	0.1	2.7	51.0	1.7	27.7	131.0	450.8	27.9	57.1	6.84	25.80	4.98	0.91	5.02	0.74	4.68	0.96	2.90	0.43	3.13	0.45	**1.178**
WB2	<0.1	11.4	0.1	2.9	57.0	1.5	27.6	104.0	456.8	32.5	66.8	8.01	31.50	5.6	1.02	5.29	0.81	4.74	1.00	3.11	0.45	3.02	0.46	**1.118**
SZ1	0.1	12.3	0.3	3.2	107.0	1.9	25.1	126.0	241.3	32.3	66.4	7.86	30.40	5.56	1.11	5.21	0.75	4.80	0.92	2.70	0.41	2.59	0.41	**1.579**
SZ2	<0.1	13	0.3	3.6	110.0	1.7	31.2	88.0	322.6	35.1	85.1	8.99	33.40	6.63	1.35	6.53	0.95	5.68	1.15	3.50	1.49	3.20	0.52	**1.428**
KU1	<0.01	10.1	0.1	2.5	46.0	1.3	30.4	124.0	560.8	30.1	61.7	7.46	28.40	5.67	0.99	5.29	0.62	5.04	1.06	3.29	0.50	3.24	0.51	0.991
KU2	<0.01	10.7	0.1	2.8	51.0	1.1	31.3	73.0	595.8	31.4	65.4	8.04	30.30	5.69	1.06	5.64	0.85	5.41	1.12	3.39	0.48	3.39	0.52	0.921
LI1	<0.1	12	0.2	3.4	112.0	2.8	26.1	96	313.7	35.0	79.8	8.17	29.50	5.59	1.03	4.67	0.77	4.84	0.95	2.87	0.46	3.06	0.46	**1.356**
LI2	<0.1	12.4	0.1	3.1	122.0	2.1	22.6	84	257.3	33.3	74.9	7.85	28.10	4.99	1.00	4.27	0.72	4.26	0.89	2.68	0.42	2.70	0.44	**1.344**
ZU1	<0.1	11	0.1	3.0	44.0	1.8	29.7	49.0	612.2	31.2	65.4	7.58	27.30	5.33	0.93	5.01	0.80	5.17	1.08	3.31	0.50	3.42	0.53	0.441
ZU2	<0.1	11.8	0.1	3.4	47.0	1.8	30.3	40.0	657.4	32.9	70.0	8.09	30.20	5.66	0.92	5.39	0.82	5.15	1.10	3.41	0.49	3.38	0.52	0.657

* elements used in PLI calculation. ** in ppb. *** in bold—values higher than 1.0.

The Pollution Load Index (PLI) values were calculated according to Tomlinson et al.'s [30] formula, taking into account the content of Cd, Cr, Cu, Pb, Zn, Co, Ni, and As in the soil samples and in the upper continental crust as background (values from Reference [10]). The highest PLI values were obtained for the soil samples from Szczurowa situated relatively far from the Steel Plant and Limanowa, which is a site distant from the industrial emission sources. Higher content of the listed elements in the area of Limanowa and Szczurowa can be caused by local emissions related to coal and wood burning, or the use of fertilizers. Differences could be related to different chemical characteristics of parent rocks. For seven sites, higher PLI values were noted for samples from the upper horizon (0–10 cm) compared with samples from the lower horizon (20–40 cm) but, for three sites, the opposite regularity was determined (Table 2).

Anthropogenic chemical contamination is often considered as a factor suitable to help defining the Anthropocene [7]. In case of the studied samples, the correlation between the concentration of elements potentially related to industrial emission. In addition, distance to industrial plants is not visible.

3.3. Magnetic Properties of Soil Samples and Mössbauer Spectroscopy

Results of magnetization measurements at room temperature (see Figure 2) show significant differences depending on the sampling site. Samples collected at a vicinity of the industrial activity sites exhibit a ferromagnetic behaviour. The ferromagnetic contribution diminishes significantly as the distance to the industrial site grows. The samples collected away from the industrial plants show very little or no ferromagnetic-like signal exhibiting rather paramagnetic behaviour. In addition, there is a relation between the intensity of the signal and the profile depth. For all the samples showing a ferromagnetic signal, the material collected at a deeper ground layer shows much less ferromagnetic phase contribution. For the paramagnetic samples, it is rather difficult to conclude on the depth dependence of the signal since its value is very low. In order to compare quantitatively, the strength of the magnetic signal among the samples and their saturation magnetization was estimated (in emu/g) by subtracting the paramagnetic contribution and taking the value of the magnetization at a maximum applied field.
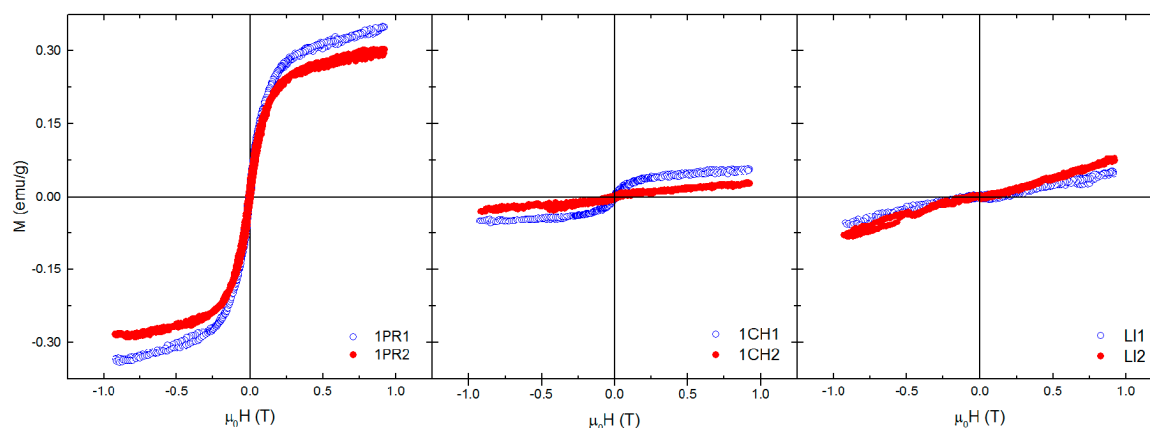

Figure 2. Magnetization loops measured on the samples from sites situated near the steel plant (**left**), at a moderate distance (**centre**) and away from the industrial plants (**right**). Blue (open) symbols denote samples collected down to 10 cm depth and red (closed) ones from 20–40 cm.

In order to check if any phase present in the sample becomes ferromagnetic at low temperatures, and, therefore, get the information necessary to elucidate the possible Fe compounds present in the material, two samples have been selected to perform magnetization versus temperature and magnetization and versus a magnetic field at different temperature measurements. As can be seen in Figure 3, there is no visible ferromagnetic contribution down to about 4 K. Only at such a low temperature can some weak ferromagnetic signals be seen.
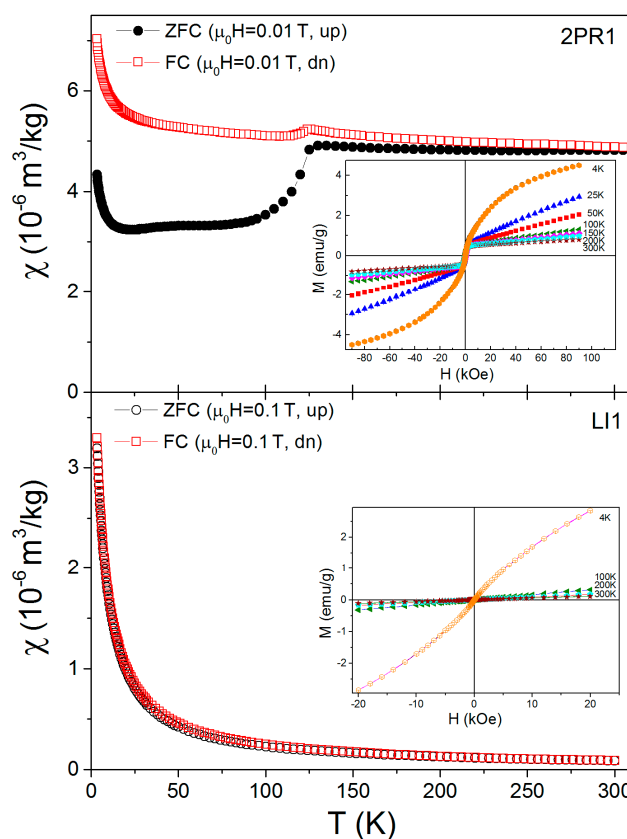
Figure 3. Magnetic susceptibility versus temperature for 2PR1 (**upper**) and LI1 (**lower**) samples. In the inset, magnetization versus applied magnetic field loops at different temperatures is shown (for symbols of samples see chapter 2. Experiments).

Results of the Mössbauer spectroscopy measurements at room temperature are in good agreement with the magnetization measurements showing a lack of any magnetic splitting in the spectra of samples from Limanowa, Wola Batorska, and Szczurowa (they could be successfully fitted with just two doublet components). Hyperfine interaction parameters point toward a presence of silicates and clay minerals [24–26] as well as an important contribution from β-FeOOH. The rest of the samples require two doublet and one or two sextet components in order to fit the spectra in a satisfactory manner. One can easily distinguish two very different groups of samples. One with a relatively low contribution of magnetically aligned Fe moments (Zawadka Uszewska, Kuchary, and Chełm) and a second one in which the magnetic phase signal is 3–5 times stronger than in the previous one (Łąki Nowochuckie, Przylasek Rusiecki 1 and 2, Wzgórza Krzesławickie). In the former case, among the silicates and clays mentioned before, a minor (usually of 6%) contribution of partly oxidised Fe_3O_4 appears. The samples with a strong magnetic signal in the case of Łąki Nowochuckie reveal the presence of Fe_3O_4, α-Fe_2O_3, and goethite (α-FeOOH), in agreement with published data [26].

In Figure 4, two Mössbauer spectra measured at room temperature, which is representative for the two groups described above, are presented. In the top panel (Przylasek Rusiecki 2), the experimental data is fitted with magnetite (Fe^{2+} and Fe^{3+}) and two silicate (Fe^{2+} and Fe^{3+}) contributions. This result is in good agreement with previous studies by other groups as discussed earlier. In the bottom panel, the spectra of the Limanowa sample are presented together with a fit assuming silicate (Fe^{3+}) and β-FeOOH contributions, as mentioned before.
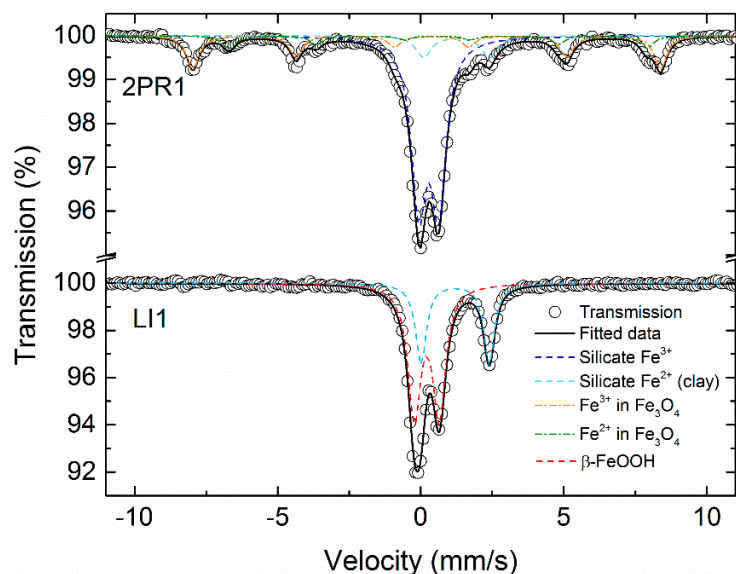
Figure 4. Mössbauer spectra measured at room temperature for 2PR1 and LI1 samples.

Interestingly, plotting the saturation magnetization versus the Fe content shown in Figure 5, one can distinguish two different types of samples. In the first case, saturation magnetization is strongly dependent on the Fe content. In the second one, the maximum magnetization measured is close to zero, even if the Fe content is high. Two previously mentioned regimes can be fitted with a linear function of the saturation magnetization (M_S) dependent on the iron content ($Fe_\%$): $M_S = a \cdot Fe_\% + M_0$, a being the proportionality coefficient, and M_0 being the saturation magnetization at null iron content. The linear regression parameters are $a = 0.15$ and $a = -0.0025$ in the latter case. A very similar trend is observed in the Mössbauer spectroscopy results when a magnetic phase contribution is plotted against the Fe content (see the inset in Figure 5). Linear regression points toward an existence of two very different forms of iron occurrence in the samples investigated giving $a = 8.6$ for the first group and $a = -1.44$ for the second group of samples.
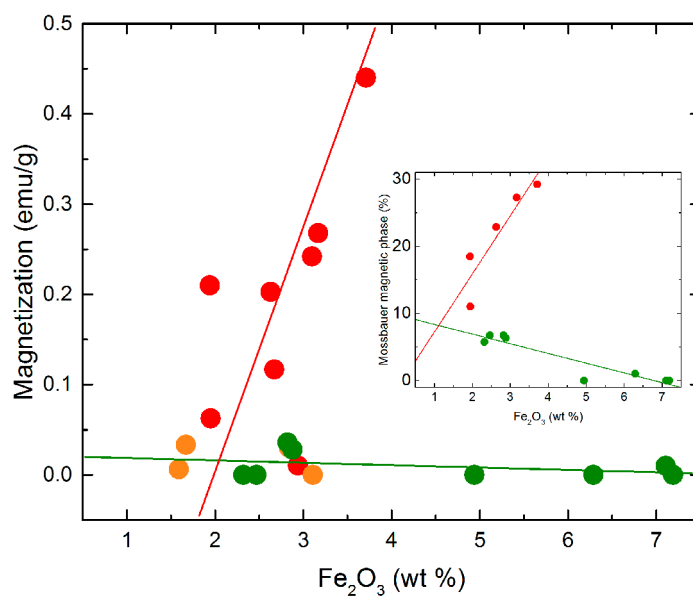

Figure 5. Saturation magnetization (main panel) and percentage of a magnetic phase derived from Mössbauer spectra fits (inset), plotted against the Fe concentration. Colours of the point correspond to colours of sampling sites (Figure 1).

3.4. Magnetic Fraction Characteristics

The content of magnetic fraction in the 20 soil samples varies from below 0.1 to 10.87 wt% (Table 3). The highest value was noted in the sample from the Łąki Nowohuckie site (sample LN1, upper level) and it is not possible to exclude accumulation of magnetic slag fragments during earthworks.

Table 3. Content of the magnetic fraction in soil samples.

Sample	Content of Magnetic Fraction (wt%)	Sample	Content of Magnetic Fraction (wt%)
1PR-1	0.90	WB-1	0.19
1PR-2	0.90	WB-2	0.03
2PR-1	4.80	SZ-1	0.06
2PR-2	0.60	SZ-2	0.03
WK-1	2.27	KU-1	0.70
WK-2	1.55	KU-2	0.29
LN-1	10.87	1LI-1	0.09
LN-2	1.16	1LI-2	0.07
1CH-1	0.30	ZU-1	0.03
1CH-2	0.10	ZU-2	0.05

In the X-ray diffraction analyses of the samples of magnetic fractions from sites situated near the Steel Plant (Przylasek Rusiecki, Wzgórza Krzesławickie, and Łąki Nowohuckie), it is possible to identify magnetite and hematite (Figure 6A). In other samples of magnetic fraction, the concentration of magnetite or hematite is low (Figure 6B) or too low for identification using X-ray diffraction.
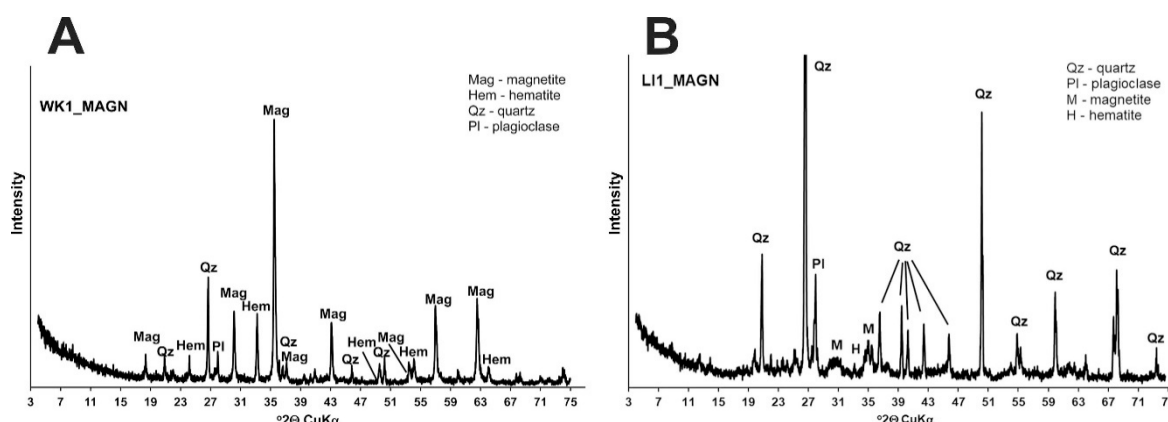

Figure 6. X-ray diffractograms of magnetic fractions. (**A**) Magnetic fraction from sample WK1 (near the Steel Plant; content of magnetic fraction – 0.70 wt%). (**B**) Magnetic fraction from sample LI1 (far from industrial plants; content of magnetic fraction – 0.09 wt%).

Using a scanning electron microscope equipped with energy dispersive spectrometry, it was possible to analyse single particles in the magnetic fraction. It was possible to notice that magnetic fractions from samples collected near industrial plants contain anthropogenic spherical grains (Figure 7A). Samples from localisations distant from industrial plants contain less spherical components but more angular ones (Figure 7B). The chemical composition of angular fragments is variable, but usually Fe and Ti dominate. The origin of this type of particles is disputable. It is possible that they represent minerals derived from a soil source rock.
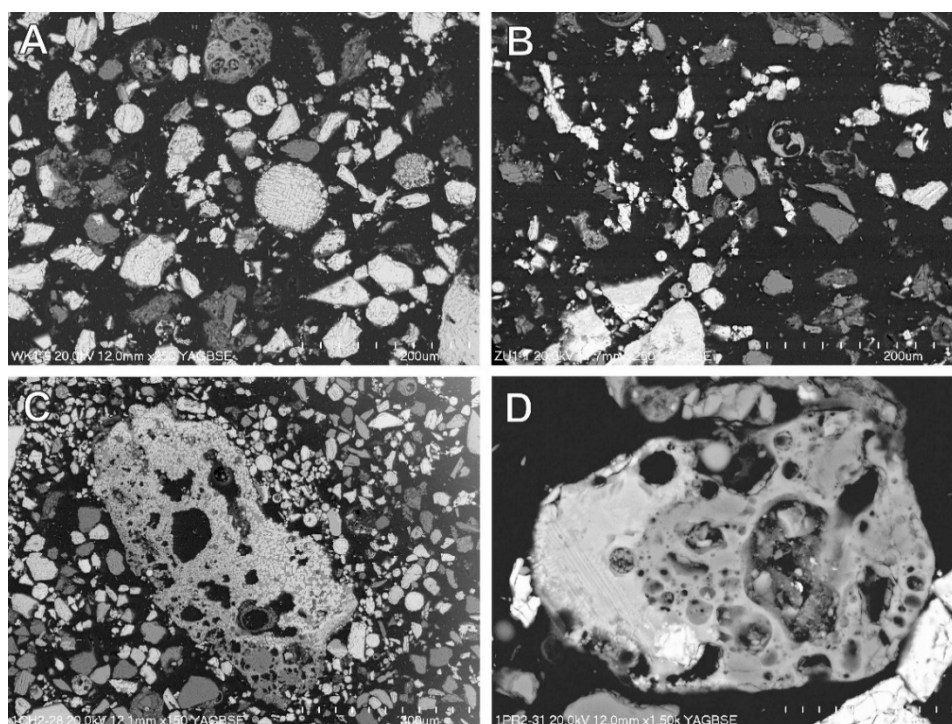
Figure 7. Magnetic fractions and their components. (**A**) Magnetic fraction from Wzgórza Krzeslawickie (site close to industrial plants) rich in spherical magnetic particles. (**B**) Magnetic fraction from Zawadka Uszewska (site distant from industrial plants) containing irregular Fe-rich particles and single small spherical Fe-rich particles. (**C**) Magnetic fraction from Chełm, small, porous, Fe oxide-rich slag fragment in the centre. (**D**) Small slag fragment in the magnetic fraction extracted from sample 1PR2.

In the magnetic fraction separated from the samples collected near the industrial plants, small slag fragments are present (Figure 7C,D). Slag fragments are vesicular and often contain Fe oxide and sometimes metallic Fe inclusions. Fe is also contained in the glassy aluminosilicate material of slag.

It is worth mentioning that, besides grains characterized by high magnetic susceptibility, the magnetic fractions also contain other magnetic components, e.g., mineral grains bound with Fe oxides (Figure 8A), soil minerals (quartz, feldspars, mica, clay minerals) aggregates with minor content of Fe oxides or Fe-Ti oxides (Figure 8B), Fe oxides or hydroxyl-oxides formed possibly during various soil processes (Figure 8C), Fe oxides, or hydroxyl-oxides formed during oxidation of pyrite framboids (Figure 8D). Fe or Fe-Ti oxides representing components of parent soil material are also present, e.g., Fe oxide containing rutile—product of weathering of biotite or hemoilmenite (Figure 8E). Anthropogenic components are also present in soil samples, e.g., aluminosilicate spherical particle of fly ash (Figure 8F), irregular fragments rich in Fe containing chromium, vanadium, zinc, and nickel (Figure 8G) or aggregates of small spherical particles such as Fe oxide particles containing Cr, Zn, Pb, and Cu (Figure 8H). Anthropogenic components could be identified because of typical shape (spherical components formed in high temperature processes), chemical composition rarely noted in rocks and soil components, or due to both factors (Figure 8F–H, respectively).
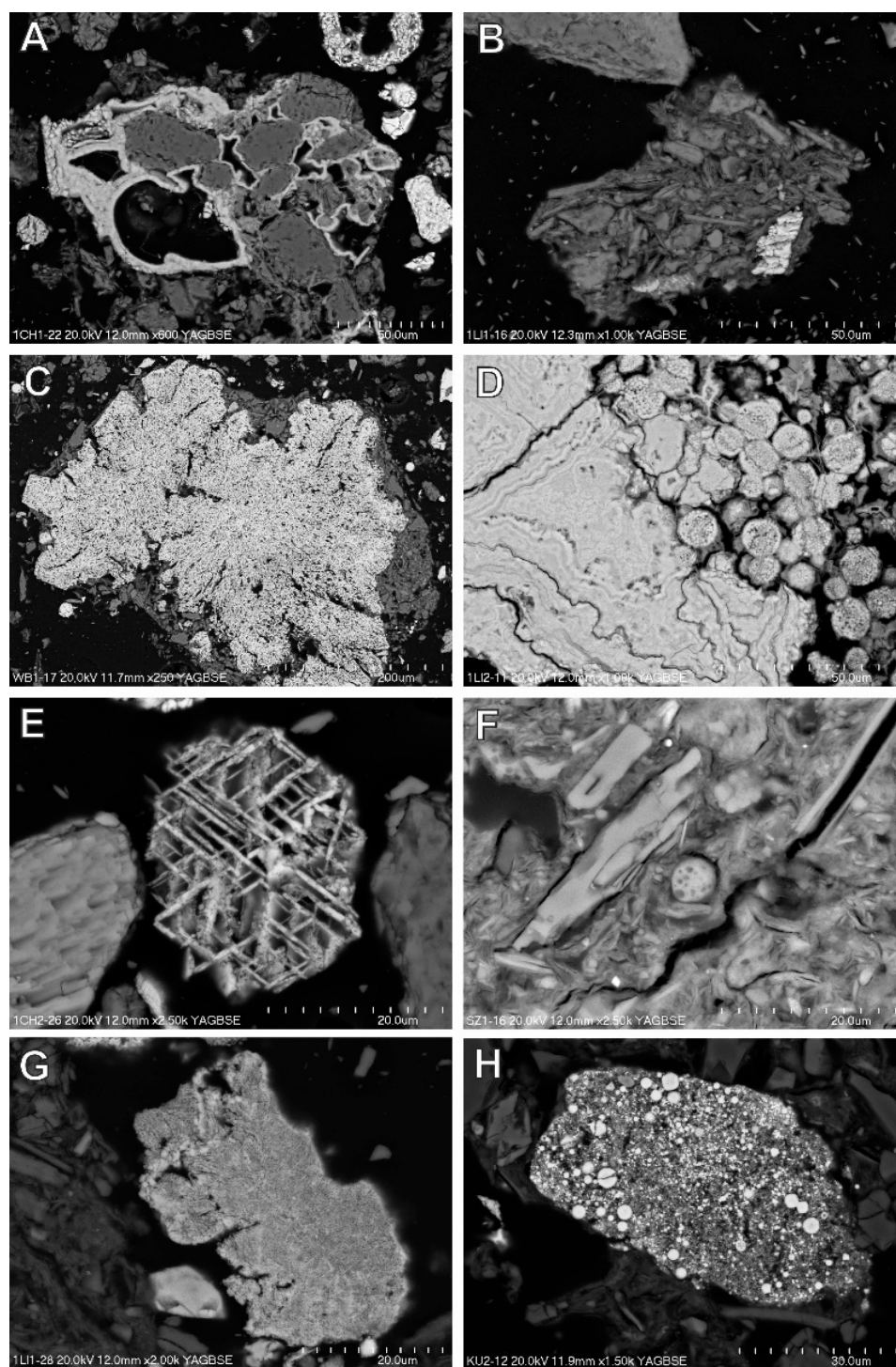
Figure 8. Magnetic fractions and their components. (**A**) Different mineral grains bound with Fe oxide, Chełm. (**B**) Aggregate with Fe-Ti oxide grain, Limanowa. (**C**) Fe oxide or hydroxyl-oxide grain, Wola Batorska. (**D**) Oxidation of pyrite framboids aggregate, Limanowa. (**E**) Fe-Ti oxide—product of weathering of minerals from parent rocks in soils, Chełm. (**F**) Fly ash spherical particle and other components in the soil aggregate. (**G**) Fe (ca 35 wt%), Cr (ca 22 wt%), Zn (ca 22 wt%), Ni (ca 3,5 wt%) oxide in magnetic fractions, Limanowa. (**H**) Aggregate of spherical particles, chemical composition—Fe from 50 to 70 wt%, Al from 0 to 1 wt%, Cr from 0 to 2 wt%, Zn from 12 to 29 wt%, Pb from 0 to 4 wt%, Cu from 0 to 0.4 wt%, Kuchary.

The Fe oxide spherules up to 30 μm in size occur in different forms. Massive Fe-rich spherules devoid of any internal structures are relatively common (Figure 9A,B). Some of them are empty with thick walls. It is possible to notice that spherules of this type are present in all samples, but their proportion to the other type is higher in the samples from Limanowa and other samples from sites distant from industrial sources. Chemical composition of massive spherules is dominated by Fe oxide but variable content of other elements is noted (Al, Cr, Si, P, Ti, Mg, Ca, K, and, more rarely, V, Zn, and Cr). Some massive spherules are composed of several single crystals of Fe oxide and contain small zones with Fe oxide exsolved in an aluminosilicate glassy matrix (Figure 9C).
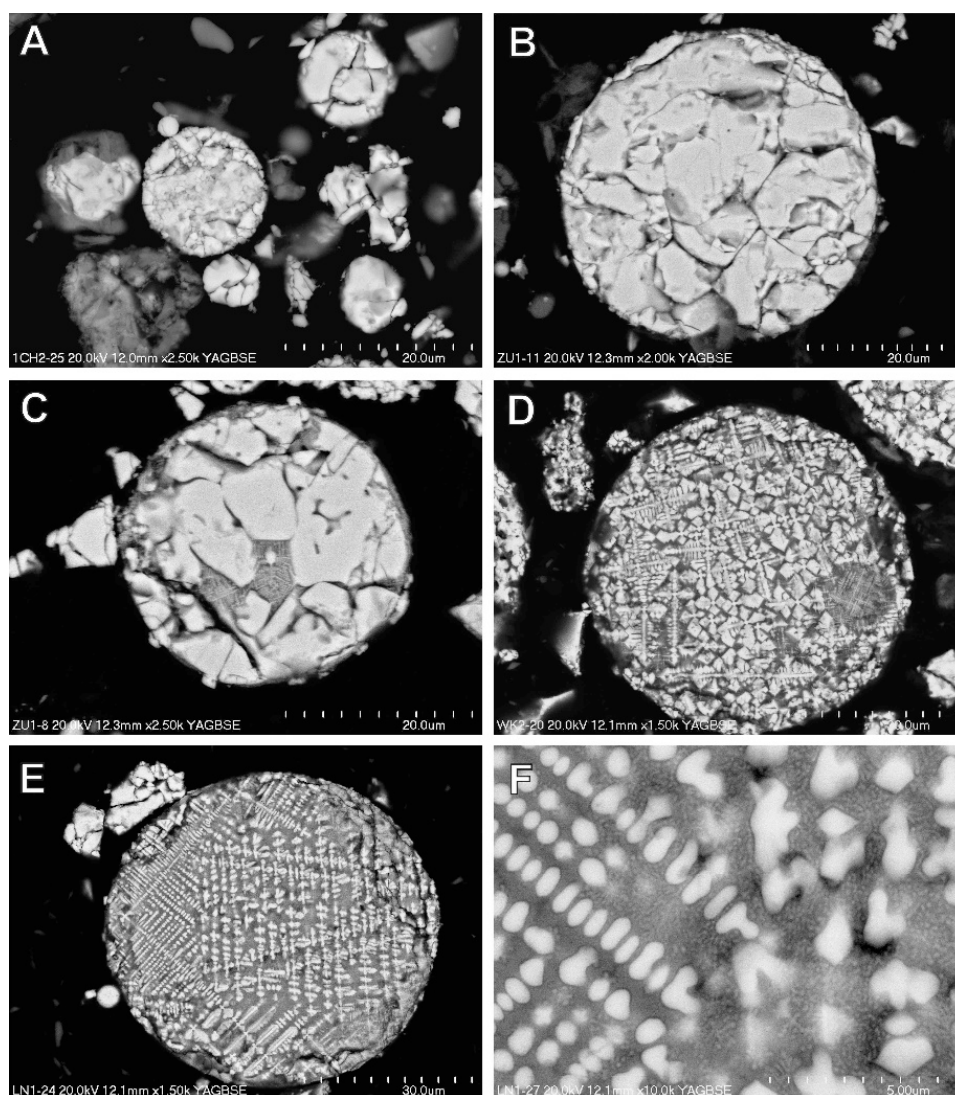

Figure 9. Spherical components of magnetic fraction. (**A**) Massive magnetic Fe oxide spherules (from 2 to 10 μm in size), Chełm. (**B**) Massive magnetic Fe oxide spherule (ca 40 μm in diameter), Zawadka Uszewska. (**C**) Massive magnetic spherule with zones composed of Fe oxides exsolved in aluminosilicate glass, Zawadka Uszewska. (**D**) Spherule with complex intergrowths of Fe oxide and aluminosilicate glass, Wzgórza Krzesławickie. (**E**) Spherule with intergrowths of Fe oxide and aluminosilicate glass. (**F**) Close-up of Figure 4E. Two size groups of Fe oxides exsolutions in aluminosilicate glass are visible.

Spherules composed of Fe oxide crystals and aluminosilicate-rich glassy material are relatively common in magnetic fractions, especially in sites situated close to industrial plants. Spherules of this type are often characterized by complex intergrowths originating from the exsolution during cooling of high temperature phases (Figure 9D). Chemical composition of both components is variable. Fe

oxide often contain Al (up to 10 wt.%, Si (up to 5 wt.%), and Ti, P, Ca, Mg, K, and, sometimes, Na. Aluminosilicate glass besides Si and Al contains Fe, P, Ca, Mg, K, and Na. Detailed investigations of intergrowths indicate that Fe-rich phase exsolutions are variable in size, ca 1–2 μm, and around 0.1 μm (Figure 9E,F).

Spherical magnetic particles with a complex internal structure contain densely packed intergrowth of elongated Fe oxide crystals with limited volume of aluminosilicate glass (Figure 10A). Several other types of magnetic spherules with a complex internal structure were noted. Particles composed of massive core and rim composed of delicate intergrowths occur rarely (Figure 10B). Magnetic spherules are sometimes composed of aggregate of isometric crystals of Fe oxide (Figure 10C), spherules containing small patchy intergrowths of Fe oxide zones in the aluminosilicate matrix (Figure 10D), and spherules with unhomogeneously distributed Fe oxides in various forms (Figure 10E,F).
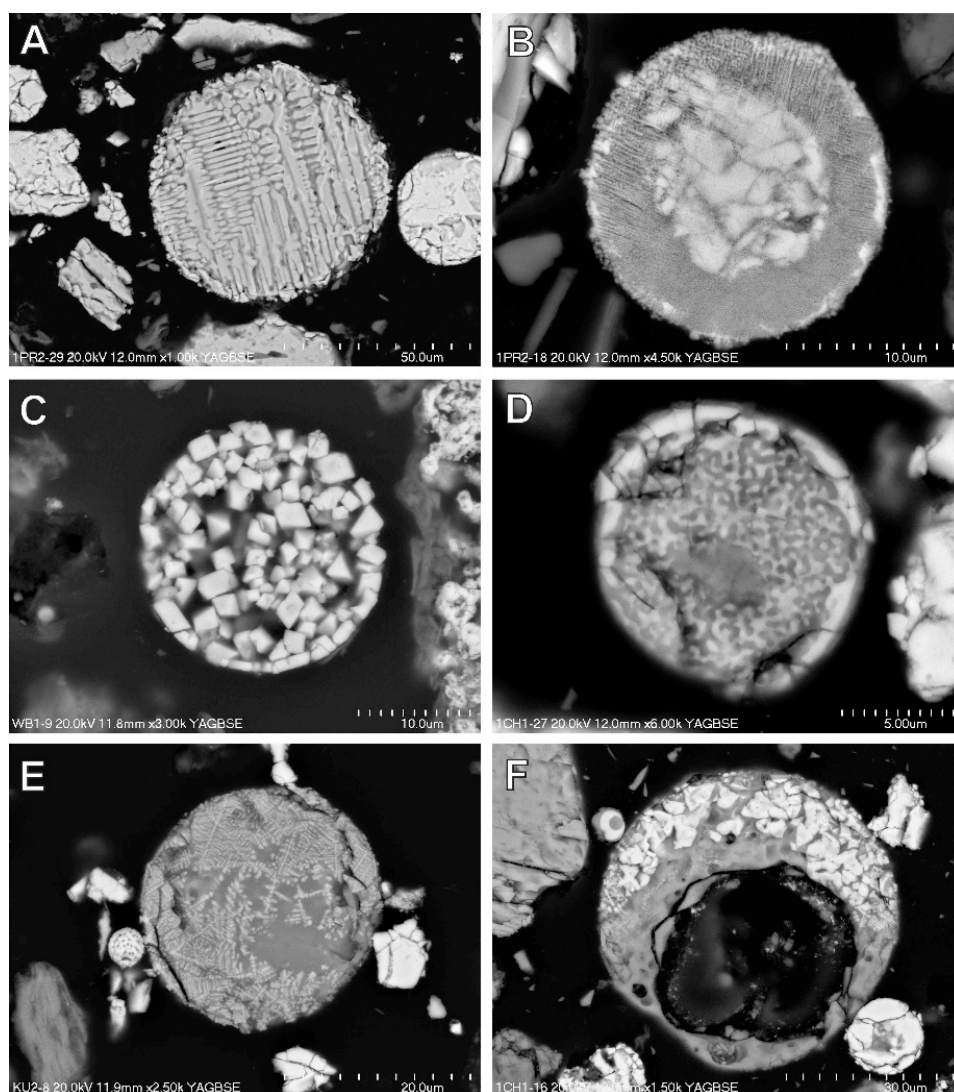

Figure 10. Spherical components of a magnetic fraction. (**A**) Spherule with intergrowths of elongated Fe oxides and aluminosilicate. (**B**–**F**) Various types of spherules.

Spherical magnetic particles in soils and sediments could be considered as an indicator of anthropogenic impact. Spherical form is considered to be related to high temperature industrial processes. A generally high temperature process in which formation of spherical particles is possible means a process realized above the melting temperature. The melting temperature depends on chemical composition of the system, flux added in the industrial process, and is usually ca 800 °C

or higher. Spherical magnetic particles originate from coal burning power plants, iron metallurgy plant, and other industrial installations. Compared with aluminosilicate spherical particles in fly ash, their identification is much easier because of simple magnetic extraction and simple identification using the SEM-EDSmethod. Spherical particles are also noted in soot emitted from some coal fired household-heating installation but the share of Fe-rich particles in soot is very low.

Magnetic spherical particles originating from power plants' fly ash were noted in soils and sediments by several authors [31,32]. The content of the magnetic fraction in the coal fly ash ranges from 2% to more than 20% [33–35]. Content of the magnetic fraction is related to coal characteristics but also to abrasion of metallic installations in power plants. Magnetic fraction of the fly ash is diversified. Smaller spheres (usually below 5 μm) are massive and sometimes hollow. Bigger spheres (usually between 10 and 80 μm in the diameter) exhibit complex internal structures ranging from Fe oxide-rich to spheres composed of complex intergrowths of Fe oxides and aluminosilicate glass. The second type is usually considered to be typical of coal-fired power plants' fly ash [36].

Spherical particles are common in dust emission from metallurgical plants. Their characteristics are strongly related to the type of ore and technology applied [37–39].

Dust from both sources (i.e., coal-fired power plants and steel works) was determined in the studied soils. Its concentration decreases with an increasing distance from industrial sources. Local emission from coal-fired household heating installations cannot be ruled out, but spherical particles in soot emitted are determined only in some of them. Spherical particles from these sources are dominated by Si and Al glass (with relatively low content of other elements). Fe-rich spherical particles occur rarely.

A difference in concentration of anthropogenic magnetic spherules (derived from steel works or power plants) in urban and suburban topsoil were described by Reference [40]. Despite differences in concentration related to the distance of sources, the results indicate the wide range aerial dispersion of industrial dust.

Because concentration of spherical magnetic particles in studied soils is not correlated with a chemical index of soil pollution (Pollution Load Index, PLI), it is possible to consider them as a better proxy of anthropogenic pollution.

4. Conclusions

All the soil samples studied contain anthropogenic magnetic particles, their identification is simple for the spherical forms that originated from high-temperature processes (e.g., solid fuel burning and metallurgy).

The content of the anthropogenic magnetic particles is higher in the samples collected near industrial plants, but is not correlated with the total Fe content in the soil or with a Pollution Load Index value. This finding is further supported by the results obtained on the basis of magnetization and Mössbauer spectroscopy measurements. We have shown the magnetic properties are not dependent on Fe content, but are strongly related to the vicinity of the industrial plants.

The results indicate the long distance (tens of kilometers) airborne transportation of coarse and high-density metallic particles from industrial plants.

We can consider the easily distinguishable anthropogenic particles in the magnetic fraction of soils as a useful marker of the post-Second World War rapid industrialisation, referred to as the "Great Acceleration" and often considered as the beginning of the Anthropocene.

References

1. Crutzen, P.J.; Stoermer, E.F. The "Anthropocene". *Glob. Chang. Newsl.* **2000**, *41*, 17–18.
2. Crutzen, P.J. Geology of mankind. *Nature* **2002**, *415*, 23. [CrossRef] [PubMed]
3. Zalasiewicz, J.; Waters, C.N.; Williams, M.; Barnosky, A.D.; Cearreta, A.; Crutzen, P.; Ellis, E.; Ellis, M.A.; Fairchild, I.J.; Grinevald, J.; et al. When did the Anthropocene begin? A mid-twentieth century boundary level is stratigraphically optimal. *Quat. Int.* **2015**, *383*, 196–203. [CrossRef]
4. Zalasiewicz, J.; Kryza, R.; Williams, M. The mineral signature of the Anthropocene in its DEEP-time Context. In *A Stratigraphical Basis for the Anthropocene*; Waters, C.N., Zalasiewicz, J.A., Williams, M., Ellis, M.A., Snelling, A.M., Eds.; Geological Society: London, UK, 2014; Volume 395, pp. 109–117.
5. Zalasiewicz, J.; Waters, C.; Williams, M.; Aldridge, D.C.; Wilkinson, I.P. The stratigraphical signature of the Anthropocene in England and its wider context. *Proc. Geol. Assoc.* **2018**, *129*, 482–491. [CrossRef]
6. Goudie, A.S. Dust storms: Recent developments. *J. Environ. Manag.* **2019**, *90*, 89–94. [CrossRef] [PubMed]
7. Gałuszka, A.; Migaszewski, Z.M.; Zalasiewicz, J. Assessing the Anthropocene with geochemical methods. In *A Stratigraphical Basis for the Anthropocene*; Waters, C.N., Zalasiewicz, J.A., Williams, M., Ellis, M.A., Snelling, A.M., Eds.; Geological Society: London, UK, 2014; Volume 395, pp. 221–238.
8. Gałuszka, A.; Migaszewski, Z.M.; Namieśnik, J. The role of analytical chemistry in the study of the Anthropocene. *Trends Anal. Chem.* **2017**, *97*, 146–152. [CrossRef]
9. Marx, S.K.; Rashid, S.; Stromsoe, N. Global-scale patterns in anthropogenic Pb contamination reconstructed from natural archives. *Environ. Pollut.* **2014**, *213*, 283–298. [CrossRef]
10. Rudnick, R.L.; Gao, S. The composition of the continental crust. In *Treatise on Geochemistry–The Crust*; Rudnick, R.L., Holland, H.D., Turekian, K.K., Eds.; Elsevier: Oxford, UK, 2003; pp. 1–64.
11. Waters, C.N.; Zalasiewicz, J.; Summerhayes, C.; Fairchild, I.J.; Rose, N.L.; Loader, N.J.; Shotyk, W.; Cearreta, A.; Head, M.J.; Syvitski, J.P.M.; et al. Global Boundary Stratotype Section and Point (GSSP) for the Anthropocene Series: Where and how to look for potential candidates. *Earth Sci. Rev.* **2018**, *178*, 379–429. [CrossRef]
12. Oldfield, F. Can the magnetic signatures from inorganic fly ash be used to mark the onset of the Anthropocene? *Anthr. Rev.* **2015**, *2*, 3–13. [CrossRef]
13. Wilczyńska-Michalik, W.; Michalik, J.; Zimirska, A.; Kuca, A.; Dietrich, A.; Michalik, M. Magnetic technoparticles in soil as a record of Anthropocene. In Proceedings of the Goldschmidt2017 Abstract, Paris, France, 13–18 August 2017.
14. Lu, S.G.; Bai, S.Q. Study on the correlation of magnetic properties and heavy metals content in urban soils of Hangzhou City, China. *J. Appl. Geophys.* **2016**, *60*, 1–12. [CrossRef]
15. Magiera, T.; Mendakiewicz, M.; Szuszkiewicz, M.; Jab, M.; Chróst, L. Science of the Total Environment Technogenic magnetic particles in soils as evidence of historical mining and smelting activity: A case of the Brynica River Valley, Poland. *Sci. Total Environ.* **2016**, *566–567*, 536–551. [CrossRef] [PubMed]
16. Łuczak, K.; Kusza, G. Magnetic Susceptibility in the Soils along Communication Routes in the Town of Opole. *J. Ecol. Eng.* **2019**, *20*, 234–238. [CrossRef]
17. Magiera, T.; Go, B.; Jab, M. Technogenic Magnetic Particles in Alkaline Dusts from Power and Cement Plants. *Water Air Soil Pollut.* **2013**, *224*, 1389. [CrossRef] [PubMed]
18. Szuszkiewicz, M.; Łukasik, A.; Magiera, T.; Mendakiewicz, M. Combination of geo- pedo- and technogenic magnetic and geochemical signals in soil profiles - Diversification and its interpretation: A new approach. *Environ. Pollut.* **2016**, *214*, 464–477. [CrossRef]
19. Thompson, R. *Environmental Magnetism*; Allen & Unwin: London, UK, 1986.
20. Singer, M.J.; Fine, P. Pedogenic Factors Affecting Magnetic Susceptibility of Northern California Soils. *Soil Sci. Soc. Am. J.* **1989**, *53*, 1119. [CrossRef]
21. Loveland, P.J. Magnetic susceptibility of soil: An evaluation of conflicting theories using a national data set. *Geophys. J. Int.* **1996**, *127*, 728–734.

22. Gangas, N.; Simopoulos, A.; Kostikas, A.; Yassoglou, N.; Filippakis, S. Mössbauer Studies of Small Particles of Iron Oxides in Soil. *Clays Clay Miner.* **1973**, *21*, 151–160. [CrossRef]

23. Mijovilovich, A.; Saragovi, C. Evidences of the stability of magnetite in soil from Northeastern Argentina by Mössbauer spectroscopy and magnetization measurements. *Phys. B Condens. Matter* **2004**, *354*, 373–376. [CrossRef]

24. Jeleńska, M.; Hasso-Agopsowicz, A.; Kopcewicz, B. Thermally induced transformation of magnetic minerals in soil based on rock magnetic study and Mössbauer analysis. *Phys. Earth Planet. Inter.* **2010**, *179*, 164–177. [CrossRef]

25. Necula, C.; Panaiotu, C.; Schinteie, G.; Palade, C.; Kuncser, V. Reconstruction of superparamagnetic particle grain size distribution from Romanian loess using frequency dependent magnetic susceptibility and temperature dependent Mössbauer spectroscopy. *Glob. Planet. Chang.* **2015**, *131*, 89–103. [CrossRef]

26. Kopcewicz, B.; Kopcewicz, M. Ecological aspects of Mössbauer study of iron-containing atmospheric aerosols. *Hyperfine Interact.* **2000**, *126*, 131–135. [CrossRef]

27. Lu, S.; Yu, X.; Chen, Y. Science of the Total Environment Magnetic properties, microstructure and mineralogical phases of technogenic magnetic particles (TMPs) in urban soils: Their source identification and environmental implications. *Sci. Total Environ.* **2016**, *543*, 239–247. [CrossRef] [PubMed]

28. Matuszko, D.; Piotrowicz, K.; Kowanetz, L. Klimat [Climate]. In *Natural Environment of Krakow, Resources–Protection–Management*; Baścik, M., Degórska, B., Eds.; Institute of Geography and Spatial Management, Jagiellonian University in Krakow: Kraków, Poland, 2015; pp. 81–108.

29. Garścia, E. Wprowadzenie do dyskusji. In *Problemy Ekologiczne Krakowa, 18, Atmosfera nad Krakowem, Przeszłość, Teraźniejszość, Przyszłość*; Wydawnictwa AGH: Kraków, Poland, 1995; pp. 33–35.

30. Tomlinson, D.L.; Wilson, J.G.; Harris, C.R.; Jeffrey, D.W. Problems in the assessment of heavy-metal levels in estuaries and the formation of a pollution index. *Helgoländer Meeresunters.* **1980**, *33*, 566–575. [CrossRef]

31. Locke, G.; Bertine, K.K. Magnetite in sediments as an indicator of coal combustion. *Appl. Geochem.* **1986**, *1*, 345–356. [CrossRef]

32. Veneva, L.; Hoffmann, V.; Jordanova, D.; Jordanova, N.; Fehr, T. Rock magnetic, mineralogical and microstructural characterization of fly ashes from Bulgarian power plants and the nearby anthropogenic soils. *Phys. Chem. Earth* **2004**, *29*, 1011–1023. [CrossRef]

33. Vu, D.-H.; Bui, H.-B.; Kalantar, B.; Bui, X.-N.; Nguyen, D.-A.; Le, Q.-T.; Do, N.-H.; Nguyen, H. Composition and Morphology Characteristics of Magnetic Fractions of Coal Fly Ash Wastes Processed in High-Temperature Exposure in Thermal Power Plants. *Appl. Sci.* **2019**, *9*, 1964. [CrossRef]

34. Murtha, M.J.; Burnet, G. The Magnetic Fraction of Coal Fly Ash: Its Separation, Properties, and Utilization. *Proc. Iowa Acad. Sci.* **1978**, *85*, 10–13.

35. Li, J.; Zhu, J.; Qiao, S.; Yu, Z.; Wang, X.; Liu, Y.; Meng, X. Processing of coal fly ash magnetic spheres for clay water flocculation. *Int. J. Miner. Process.* **2017**, *169*, 162–167. [CrossRef]

36. Valeev, D.; Kunilova, I.; Alpatov, A.; Varnavskaya, A.; Ju, D. Magnetite and Carbon Extraction from Coal Fly Ash Using Magnetic Separation and Flotation Methods. *Minerals* **2019**, *9*, 320. [CrossRef]

37. Wilczyńska-Michalik, W. Z badań mineralogicznych pyłów emitowanych przez Hutę im. Lenina w Krakowie [Mineralogical study of dusts emitted from the Lenin Steel Plant in Kraków]. *Prace Mineralogiczne PAN* **1981**, *68*, 1–57.

38. Muszer, A. Mineralogical characteristics of metallurgical dust in the vicinity of Głogów. *Physicochem. Probl. Miner. Process.* **2004**, *38*, 329–340.

39. Csavina, J.; Taylor, M.P.; Félix, O.; Rine, K.P.; Sáez, A.E.; Betterton, E.A. Size-resolved dust and aerosol contaminants associated with copper and lead smelting emissions: Implications for emissions management and human health. *Sci. Total Environ.* **2014**, *493*, 750–756. [CrossRef] [PubMed]

40. Yang, T.; Liu, Q.; Zeng, Q.; Chan, L. Relationship between magnetic properties and heavy metals of urban soils with different soil types and environmental settings: Implications for magnetic mapping. *Environ. Earth Sci.* **2012**, *66*, 409–420. [CrossRef]